Crosstalk reduction in a piezoelectric phononic plate induced by electrical boundary conditions: Application to multi-element transducers

L. Fei, Lionel Haumesser, L.-P. Tran-Huu-Hué

Version of Record: https://www.sciencedirect.com/science/article/pii/S0041624X21002559
Manuscript_41217cf2cdd69bf96cf63ed4606117fa

Crosstalk reduction in a piezoelectric phononic plate induced by electrical boundary conditions: application to multi-element transducers

L. Fei[1] **L. Haumesser[1,*]** **L.-P. Tran-Huu-Hué[1]**

[1] *GREMAN UMR 7347, Université de Tours, INSA Centre Val de Loire, 3 rue de la Chocolaterie, 41000 Blois, France*

*lionel.haumesser@univ-tours.fr

Abstract

This paper proposes a method of passive electrical decoupling which aimed at found application in reducing the crosstalk phenomenon in multi-element ultrasonic transducers. A homogeneous piezoelectric plate, covered on one side by a 1D periodic arrangement of thin metallic electrodes and on the other side by a full electrode, is considered. Finite element analysis and experimental measurements are performed to obtain the dispersion curves and normal displacements at the surface of the structure. It is shown that applying inductive shunts at the electrodes, band gaps can be created in the first Brillouin zone, which can prevent from the establishment of the first thickness mode in the plate. In that way the mechanical inter-element coupling can be lowered. Thus, the acoustic radiation in water from one sector excited at the resonance frequency is found to be closer to that of a piston mode. The transposition of this principle to the situation of a transducer including a rear medium and a front matching layer confirms the possibility of reducing the inter-element coupling. However, the physical effects at the origin of this reduction are different from those inherent to the cutting of a piezocomposite ceramic as it is done in most probes available in the market. As a result, we show that taking advantage of the electrical boundary conditions upon the passive elements in a transducer gives real opportunities for crosstalk reduction that may be implemented in ultrasonic systems for imaging in the medical field and in NDT.

Keywords: Crosstalk, Piezoelectric phononic crystal, Multi-element transducers

1. Introduction

Multi-element piezoelectric ultrasonic transducers are widely used in medical or industrial field due to their ability to detect shape flaws of any kind without mechanical movement of the probe [1–6]. This feature is linked to the possibility of independent control of the elements of the transducer. For this reason, among the many conditions to be fulfilled for having a good quality of the ultrasound image, the crosstalk should be maintained at a low level.

The crosstalk corresponds to the coupling possibly mechanical, acoustic, and electrical, between the elements in a multi-element transducer. It tends to increase the number of vibrating elements by comparison to the number of electrically excited (active) elements, produces spurious guided modes in the array, that may cause disturbances in the acoustic radiation. As a result, it can create artifacts or masks sharp details in the image due to extra lobes in the radiation pattern. For electronically focused systems, it can also disrupt the focus by enlarging the focal spot. Another undesirable effect of crosstalk is an increase in response time and thus a reduction in bandwidth. To disable the crosstalk phenomenon, guided and stationary waves should be avoided in the piezoelectric plate. The main idea is to make the electrically excited elements vibrate locally and isolated so as to obtain a radiation pattern as wide as possible, as a source point under the Huygens principle.

Some solutions have been proposed to reduce this drawback. For example, a passive mechanical decoupling between the elements can be achieved by the periodic dicing of the piezoelectric ceramics, such as piezocomposites [7–10]. The design leads to lower crosstalk by creating a wide band gap for elastic waves around the working frequency [11]. Another kind of solution is active electrical decoupling [12]. Using this procedure, it consists in applying to the other elements, except to the active one, an appropriate electrical voltage so as to minimize the displacement field. A third approach concerns passive electrical decoupling. It is notably reported in a recent study, using grounded non-active elements [13].

At high frequencies, sub-dicing of the plate to delimit the active elements becomes hazardous due to the thickness smallness. It is the case for frequencies above 50 MHz for which kerfless transducers, e.g. without physical separation between the elements except for the electrodes, are designed [14,15]. The crosstalk effects are low for such transducers because the materials used have a thickness mode weakly coupled with lateral modes [16,17]. These materials available as thick films are unusable for working frequencies around 1 MHz, the frequency range in our study. The possibility to lower crosstalk is here considered, but only by applying specific electrical boundary conditions to the elements next to the active element, while using standard piezoelectric materials with thickness in the millimeter range, without machining mechanical notch between the elements.

In this paper, we investigate the method of passive electrical decoupling using inductive shunts connected to a piezoelectric phononic plate. The ability of passive complex periodic structures to absorb and filter vibrations, or to favor a hybrid propagation mode, has been shown recently [18,19]. Regarding the electroactive structures such as those studied in our study, previous work [20–24] have highlighted the possibility to create band gaps at the edge and within the Brillouin zones under suitable electrical boundary conditions applied to a set of periodic electrodes. The intention here is to create a band gap to the first thickness mode for the non-active elements of the plate. By localizing the normal vibration in the plate in this way, it is expected that the radiation pattern of the pressure field at this frequency can be broaden. Then the radiation pattern for a piezo composite transducer with a backing medium and a front matching layer is numerically simulated to test our solution. These elements are always present in ultrasonic arrays. They increase the bandwidth and the sensitivity but can have a large influence on the guided waves in the piezoelectric plate and eventually a negative impact on the radiation when combined with shunts. Beyond the first step described here which concerns the main element (electroactive) of a transducer, subsequent scientific and technical issues may arise when integrating it in the device by adding many front matching layers and enlarging the bandpass. It is understood that to implement such improvement for commercial transducers is a long-term objective. At the end, it can be seen as a supplementary way to reduce crosstalk effects in combination with existing technics.

The paper is organized as follow. In Sec. 2, two simulation models are introduced to obtain dispersion curves and related normal surface displacements of the guided waves in the electro-mechanical plate, in both open and shunted electrical conditions. In Sec. 3, the sample and experimental device are presented for validation of the simulation results. Then, the effects and benefit of the inductive shunts are discussed (Sec. 4): the investigation is concerned with Lamb waves propagation around the resonance frequency of the first piezoelectrically coupled thickness mode, normal surface vibration localisation and far field radiation in water. To highlight the future possibilities of the method, the solution is implemented in Sec. 5 considering the configuration of a piezocomposite transducer with sixteen elements, a backing medium and a front matching layer. Finally, Sec. 6 is the conclusion and future outlines to this work.

2. Piezoelectric phononic plate modelling

In this work, the sample studied is a two-dimensional piezoelectric Pz26 homogeneous square plate (80 * 80 mm^2) polarized across the thickness t that is equal to 2.236 mm. One side of the plate is covered by a periodic array of rectangular conductive electrodes and the other side by a full single electrode connected to the ground. The electrodes on both sides are considered as perfectly conductive surfaces whose thickness which are around one tens of microns, is neglected in comparison to the thickness of the plate. Material parameters

of Pz26 used in the computations can be found in [25]. For purpose of characterizing wave propagation in this system, the numerical models of a 2D unitary cell of an infinite piezoelectric phononic plate and that of a finite piezoelectric phononic plate having forty unitary cells, are presented in the following sub-sections.

2.1. Infinite piezoelectric phononic plate model

For the calculation of the dispersion curves for ultrasonic guided waves in the piezoelectric phononic plate, a 2D finite element model (COMSOL Multiphysics) is built. We choose an elementary cell as depicted in Fig. 1. Its width is noted a and is equal to 2 mm. It is covered with a full grounded electrode on one side and with a central electrode of width $e = a - b$ on the other side (b is the kerf between two adjacent electrodes in the phononic structure). Geometrical sizes of the electrode and the kerf are $e = 1.9$ mm and $b = 0.1$ mm, respectively. The electrode is either let at floating potential (OC: open circuit) or connected to an inductance whose other terminal is grounded (IS: inductive shunt). Floquet Periodic boundary conditions [26] are applied at $x = 0$ and $x = a$ for both the mechanical displacements and the electric potentials. Frequencies are calculated from real wavenumbers to obtain the dispersion curves in the first Brillouin zone (Fig. 2) and the modes identified by their displacement fields are also indicated.

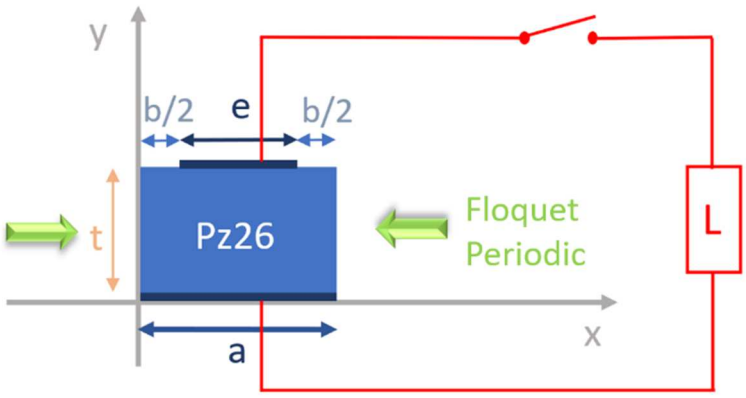

Figure 1: Unit cell model of the infinite piezoelectric phononic plate with OC (open circuit) and IS (inductively shunted) electrical boundary conditions on the electrodes.

The targeted frequency range in this work is specific to the application. The piezoelectric ultrasonic transducer typically vibrates in piston mode. Therefore, the electroactive plate vibrates in thickness mode at the first mechanical resonance frequency f_r, piezoelectrically coupled [27,28]. Considering the material and the thickness of the sample in this study, $f_r = 1.03$ MHz, which fits the theoretical value that is obtained according to the following equation (Eq. (1)),

$$f_r = \frac{1}{2t}\sqrt{\frac{C_{33}^D}{\rho}} \quad (1.)$$

where t and ρ are the thickness of the plate and the density, respectively, and C_{33}^D is the elastic coefficient along the y-axis according to the thickness.

The resonance frequency can also be observed in the dispersion curves for OC boundary condition at the cut-off frequency of the S_2 Lamb mode (red arrow in Fig. 2(a)). Adding an inductive shunt of 22 µH to the piezoelectric plate opens a band gap for the S_2 mode around f_r. The gap is comprised between frequencies f_+ and f_- noted in Fig. 2(b).

On the detailed view (left in Fig. 3), it can be observed that the band gap is not complete. In particular, the folding of the A_0 and the S_0 modes is not affected by the shunt. The inductance value is chosen within a range up to 90 µH (right in Fig. 3). The goal is to obtain the frequency range broader as possible and centred at the

resonance frequency. Following these criteria, the optimum inductance value is found to match with 22 ± 1 µH.

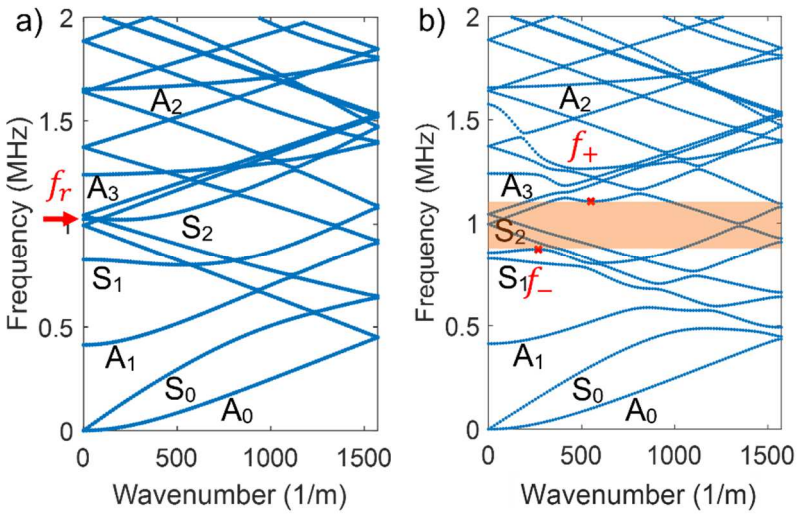

Figure 2: (a) Dispersion curves of the Lamb waves in the plate in OC condition. The thickness mode at the mechanical resonance frequency f_r is indicated by the red arrow. It corresponds to the cut-off frequency of the S_2 mode. (b) Dispersion curves of the Lamb waves in the plate in IS condition using an inductance of 22 µH; A band gap (shaded area) is created between f_+ and f_- for the S_2 mode.

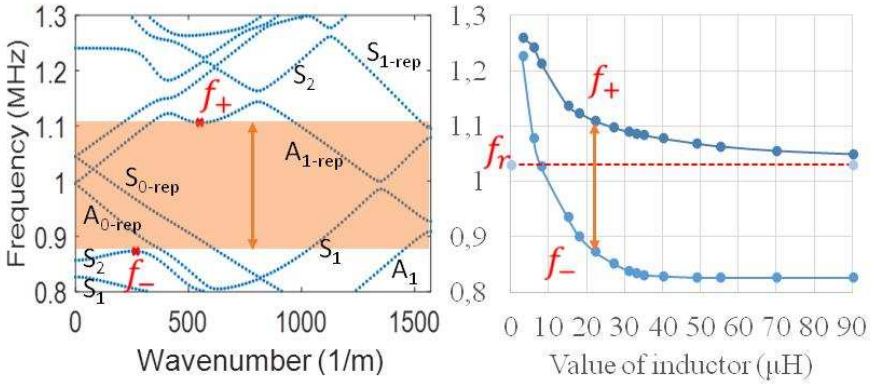

Figure 3: Detail of Fig. 2(b) for the piezoelectric phononic plate in IS boundary condition (left). Diagram of the frequencies f_+ and f_- as a function of the value of the inductance (right).

2.2. Finite piezoelectric phononic plate model

The optimum value of the inductance was determined considering the unit cell of an infinite periodic plate. Another numerical model is now introduced to take into account the finite number of unit cells of the sample. The piezoelectric plate is made of 40 cells (sectors) and has a total length of $L = 40\ a = 80$ mm. The 20th sector is excited with a harmonic voltage source and the remaining sectors are either with OC or with IS boundary condition (Fig. 4). The model is 2D in the x-y plane and the plate size along the z-direction is set to L also. Free boundary conditions are applied to the edges of the plate (at $x = 0$ and $x = L$ for $0 \leq y \leq t$). A frequency study is achieved and normal displacements at $y = t$ are obtained for any $0 \leq x \leq L$. Using this model, simulation results are more easily compared to the experimental ones and the influence of the edges of the plate can be assessed according to the voltage source location (Sec. 4).

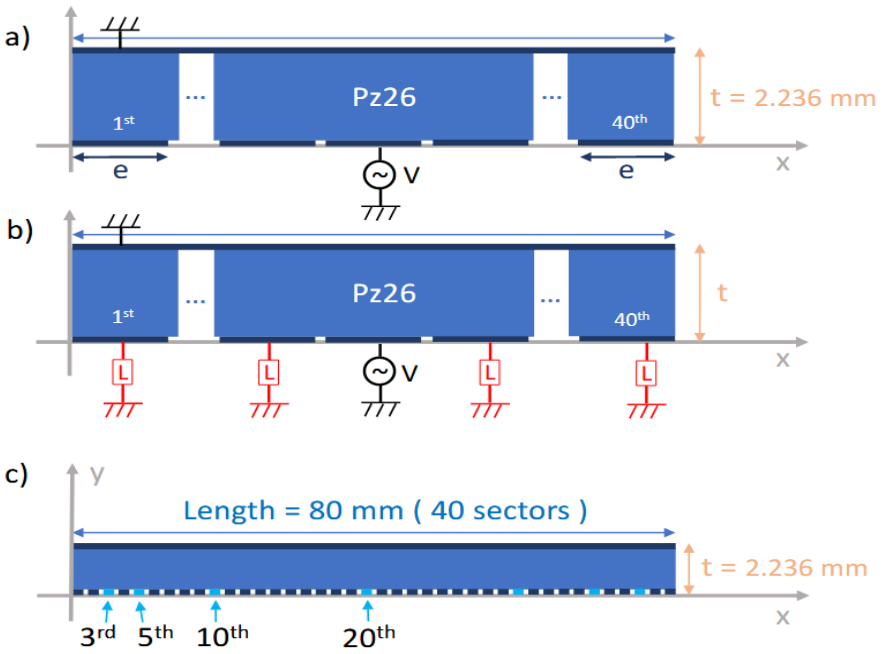

Figure 4: Two-dimensional model of the finite piezoelectric phononic plate. The 20th plate sector is excited using a harmonic voltage source. Other sectors are set to either OC (a) or IS (b) electrical boundary condition. Sector location (c).

3. Sample and experimental device

In this section, the experimental setup and data acquisition principle are presented.

In order to maintain mechanically the inductors, a holder is used (Fig. 5). The plate sectors are connected to the holder using a set of flat ribbon conductive cables. The additional impedance (Z_{add}) brought by the extra connexions was evaluated. A spectrum analyser (Omicron Lab/Bode 100) was used to measure the impedance of the inductors and the full IS (i.e., wire + inductor) connected to any sector, in the frequency range 0-2 MHz. Results show that the mean value of inductors impedance is $Z_{Lexp} = (R_{Lexp}; L_{Lexp}) = (3.21 \pm 0.16\ \Omega; 21.14 \pm 0.53\ \mu H)$.

Further, the configuration with the full IS that has the highest impedance, among the 39, is evaluated in order to deduce $Z_{add} = 1.28\ \Omega$. These values ($Z_{Lexp} + Z_{add}$) were used as new input data to re-calculate the dispersion curves and compare them to the results at left in Fig. 3. The gap for the S_2 mode is reduced by 1% for $267.0 \leq k \leq 565.5\ m^{-1}$. In the end, the influence of the extra impedance is considered weak enough so that the setup can be used in the following.

Moreover, a waveform generator is used to deliver a one period of sine burst with an amplitude of twenty volts at the frequency of one Megahertz. The excitation is applied at some sector without inductor of the plate. Due to the symmetry of the system, elastic waves mainly propagate in the *x*-*y* plane within the piezoelectric plate. Out-of-plane mechanical displacement measurements of the plate surface at the grounded electrode ($y = t$) are measured as a function of time by a single point laser vibrometer (Polytec's OFV-505). The successive A-scan type signals are collected in the *x*-direction with a 0.2 mm increment at $z = 40$ mm corresponding to the middle position on the plate. The surface of the aluminum plate has some roughness or small scratches that can locally defocus the light beam, degrading the signal to noise ratio. To limit this drawback, a thin adhesive reflective tape (0.3 mm) is deposited on the plate along the measurements path. The sub-wavelength thickness of this adhesive tape does not affect the measurement while the optical reflectivity of the plate is strongly enhanced to ensure a permanent optimal focus of the reflected beam at any point of the scanned line.

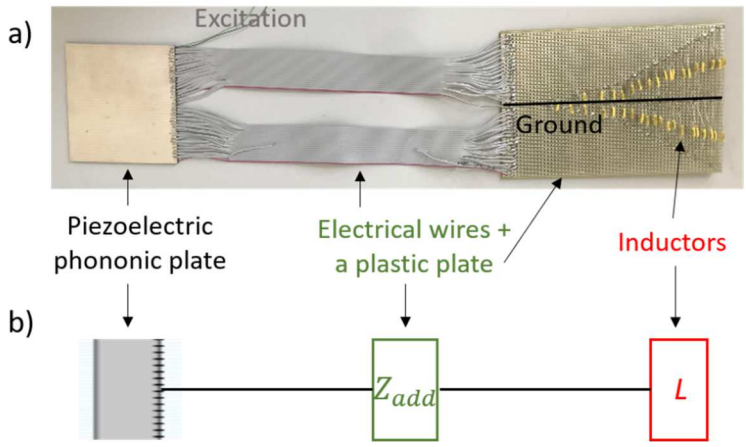

Figure 5: Photograph (a) and sketch (b) of the experimental device.

4. Results and discussion

Now we analyze the effect of the inductive shunts from the crosstalk reduction point of view in the piezoelectric phononic plate. It will successively tackle changes in the dispersion curves around the first thickness mode frequency, the normal displacement field re-distribution along the plate surface and the far field radiated pressure in water at the resonance frequency.

4.1. Propagation of Lamb waves in the piezoelectric plate

In this section the electrical voltage is applied to the first plate sector ($0 < x < 2$ mm in Fig. 4). Surface normal displacements are collected all along the x direction ($2 < x < 80$ mm). Fast Fourier Transforms are performed from these data in order to obtain the dispersion curves in the frequency / wave number representation. In any case, the duration of the processed signal at most corresponds to a one-way trip along the piezoelectric phononic plate for the propagating waves. Results are displayed for the OC and IS electrical boundary conditions, both numerically and experimentally in Fig. 6.

The main observation is concerned with the thickness mode at the frequency f_r when k is equal to zero (see in the yellow rectangle in the first Brillouin Zone - BZ). Experimentally in OC condition, it is observed at the cut-off frequency of the S_2 mode at 1.02 MHz, in agreement with the numerical value (see Sec. 2). With the IS condition, the S_2 mode vanishes at $k = 0$ m^{-1} and split for higher k in the first BZ. It resumes for higher frequencies (around $f = 1.1$ MHz) where it is observed in particular at positive wavenumber values. As a matter of fact, back travelling wave on the plate are now observed due to the impedance contrast introduced by the shunts.

Above and below the framed area is the electric mode as described elsewhere [22]. This mode is not of straight interest in our work whose targeted frequency range is around f_r. In the same way, one observes in the different Brillouin zones a lot of modifications in the trajectories of the Lamb modes, with stop bands in and at the edges of the BZs, and also mode reflections and mode conversions (a few of them are indicated by white arrow in Fig. 6). Such features can also be seen on a smaller scale considering OC conditions, since electric potentials are periodic on one face of the plate. Here again the frequency and wave number zones where this occurs are far from the area of interest targeted for this work and the changes observed there will not be detailed further.

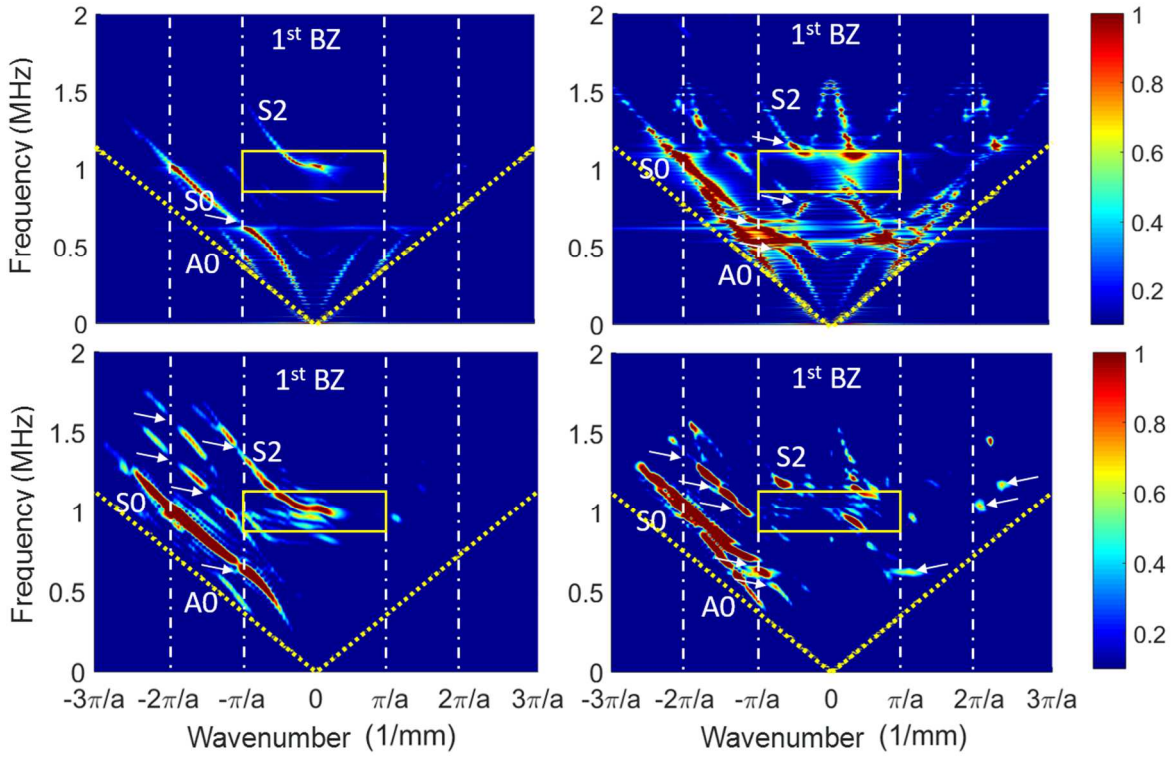

Figure 6: Simulated (top) and experimental (bottom) dispersion curves of Lamb waves in the plate with OC electrical boundary condition (left) and with IS electrical boundary condition (right). The Brillouin zones (BZ) are separated by vertical dashed lines. The frame at the center indicates the region of interest for the effect of the IS on the first thickness mode. The slope of the dotted yellow lines is the wave velocity in water.

Finally, there is an important point to emphasize for IS curves. Whatever the frequency, waves never have a lower phase velocity compared to the speed of sound in water. This contrasts with the case of waves in piezoelectric plates whose periodicity is obtained by the dice and fill process. Indeed, in this case, the waves can be subsonic [29].

In the next paragraph, we will see to what extent stopping thickness vibration in the vicinity of f_r, allows more localization of the vibration at the vicinity of the excited sector.

4.2. Distribution of normal displacements along the piezoelectric plate

By now, the electrical voltage is applied to the 20th plate sector ($38 < x < 40$ mm) and surface normal displacements at the resonance frequency are collected on the grounded side of the plate, all along the x direction. Numerical results highlight strong changes between OC and IS boundary conditions (Fig. 7).

When passive sectors are in OC condition, it is observed that the amplitudes upon the five elements on both sides of the excited element are at less than 10 dB below the level on the excited element. Therefore, it reflects a significant level of crosstalk in this region of the plate. The contribution to crosstalk from the more distant parts of the plate is less important (< -10 dB). Nevertheless, small oscillations of amplitudes resulting from round-trip guided waves are observed, which interfere in the plate whose ends are free.

The overall level is lower when passive sectors are in IS condition. It can be observed in the central region for which only the displacement fields on sectors 17 and 23 have a level greater than -10 dB, corresponding to smooth gradient of the phase, and also in remote areas for which levels are under -20 dB, corresponding to stronger gradient of the phase.

As far as the experimental readings are concerned, we find the trends described above, and the preponderance of the eleven central elements, even if the dynamic is less important, of the order of -3 dB in OC and -8 dB in IS boundary conditions. Despite the few common characteristics that have just been highlighted, the moduli of

the measured and calculated displacements are different. The numerical model makes a 2D plane strain approximation which is the main reason for the discrepancy. On the one hand, due to the size of the plate along the z-axis (80 mm), the approximation fits the propagation condition along the x-axis as can be seen in Fig. 6. This was chosen because the reduction of crosstalk is based on the analysis of wave propagation. On the other hand, the source condition which involves excitation along the z-axis of one plate sector rather meets the 2D plane stress approximation. Neither of the two approximations fully corresponds to the experimental situation which should therefore be described using a 3D model. This option could not be implemented because of the cost in numerical resources.

In the next section, the displacement fields are used to obtain the pressure far fields radiated in water.

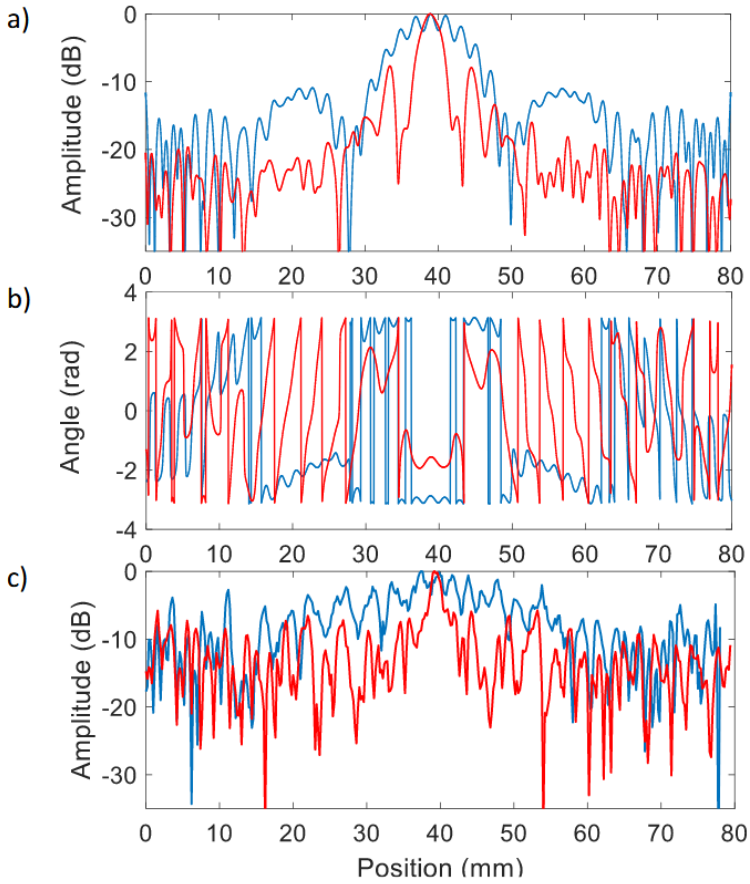

Figure 7: Normal displacement along the piezoelectric phononic plate with OC (blue line) and IS (red line) electrical boundary conditions at the resonance frequency. Simulated amplitude (a), Simulated phase (b) and experimental amplitude (c). The source sector is in the range $38 \leq x \leq 40$ mm.

4.3. Radiation diagrams analysis

The Rayleigh integral is used in the rigid baffle approximation in order to calculate the far field radiation diagrams in water [30-32] at the resonance frequency (Fig. 8). The zero angle corresponds to the y-direction (See Fig. 4). Amplitudes in dB are normalized by the maximum amplitude in each diagram.

It can be observed, even on the theoretical curves, that diagrams are not fully symmetric for positive and negative angles since the 20th element (the active one), is not at the center of the periodic array.

In OC electrical boundary condition, the radiated pattern exhibits three main lobes (Fig. 8(a)). The central lobe corresponds to the radiation of the activated element. The lateral lobes at ±48° are related to the periodicity of the grating. They appear here because the wavelength of the radiated wave in water is smaller than the grating

pitch *a*. A simplified radiation pattern of Fig. 8(a) is obtained when only taking into account contributions above -10 dB from Fig. 7 (solid blue line in Fig. 8(e)).

With the IS condition (Fig. 8(b)), the central lobe is split into two parts oriented at $\theta = \pm 6°$. This squint angle is evaluated at the maximum of the nearest lobe from 0° (apart from 0°). The angle θ as well as at this angle, the difference Φ between the pressure level and that at the 0° angle are reported in Tab.1. Another clear difference on the radiated pattern according to the electrical termination are new lobes at ±28°. It originates from the phase opposition of the 17th and 23rd sector radiation with respect to the active one. This is confirmed in the simplified pattern since the feature is observed when only considering displacement contributions of the 17th, 20th and 23rd sectors in the radiation (solid red line in Fig. 8(f)).

The experimental results are obtained from raw data without time windowing prior to processing (Fig. 8(c)-(d)). They confirm the trends announced from the numerical insights, including the broadening of the central lobe which corresponds to a reduced size of the effective radiating area with the IS termination and thus to a crosstalk reduction.

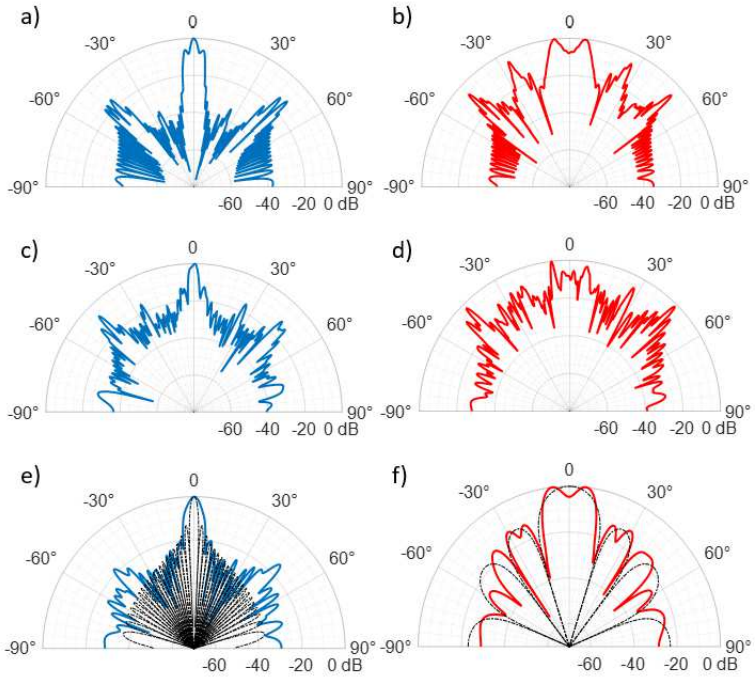

Figure 8: Simulated (top) and experimental (middle) radiation patterns from the piezoelectric phononic plate with OC (left) and IS (right) electrical boundary conditions at the resonance frequency. Simplified (from Fig. 7) and calculated (from Eq. 2) radiation patterns (bottom).

From the evaluation of the angular width of the central lobe, the effective width *D* of the radiating area (the active sector and its periphery) can be assessed using the classical formula for gratings [26]:

$$H(\theta) = \left| \frac{\sin \frac{\pi D \sin\theta}{\lambda}}{\frac{\pi D \sin\theta}{\lambda}} \right| \left| \frac{\sin \frac{N\pi a \sin\theta}{\lambda}}{N \sin \frac{\pi a \sin\theta}{\lambda}} \right| \quad (2.)$$

The *D* values obtained are shown in Tab. 1 for the two electrical terminations. The change is striking since the effective width of the radiating area is reduced by a factor of more than six with the IS termination. For more clarity, the effect of this reduction in crosstalk is again underlined by calculating *H(θ)* using Eq. 2 and from the values of *D*, then comparing the plots to the simplified diagrams (see Fig. 8(e)-(f)).

Table 1: Effective width D, squint angle θ, and accompanying pressure level difference Φ calculated from theoretical radiation patterns for the OC and IS electrical boundary conditions.

Electrical boundary condition	Effective D (mm)	θ (°)	Φ (dB)
OC	32.4	4	6
IS	4.8	6	-7

Finally, we consider the influence of the active sector position on the far field radiation at f_r. Radiation diagrams are shown for four positions considering both OC and IS boundary conditions (Fig. 9). It can be seen that when the 10th or the 5th sectors are active (see Fig. 4(c)), the slight dissymmetry that sets in does not modify the overall appearance of the observed pattern as the 20th sector is active. The effective parameters evaluated in Tab. 1 remain as it were unchanged. Nevertheless, in the IS condition when the 5th sector is active, we notice an evolution of the amplitude of the lobes at $\pm$28° and $\pm$56°. As the active sector moves closer to the edge of the array (3rd sector), the main lobe is broader regardless of electrical boundary conditions. The diagrams are no longer symmetrical with respect to 0° and effective parameters are not suitable anymore for their description. As previously said, the results are obtained applying the IS termination at each sector except the active one. However, additional calculations (bottom line in Fig. 9) show that these results remain substantially unchanged as long as there are at least four shunted sectors on either side immediately adjacent to the active sector: the effective width is then about equal to 5 mm.

We conclude here that the finite length of the array weakly affects the radiation diagram symmetry but not the broadening of the diagram. These results make sense as far as the active sector is at least at a distance from the edge of the plate equal to D/2, approximatively.

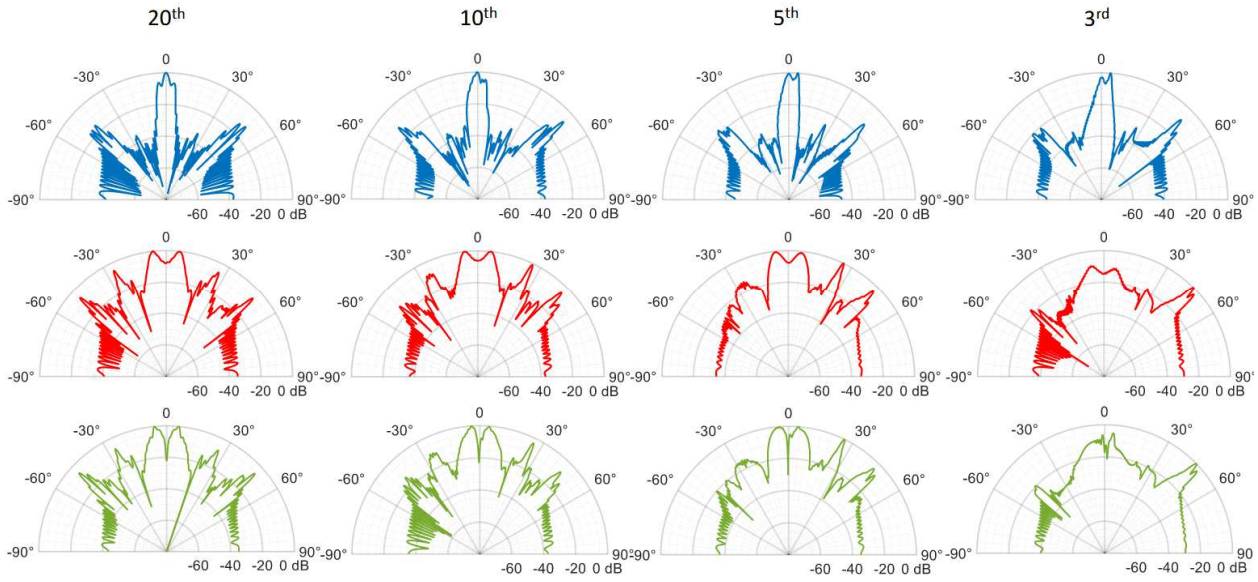

Figure 9: Radiation diagrams for four positions of the active sector: 20th, 10th, 5th, and 3rd sectors. OC electrical boundary conditions (top - blue line). IS electrical boundary conditions (middle - red line). IS electrical boundary conditions at 4 sectors adjacent to the active element (bottom - green line).

In the next section, to highlight the future possibilities of the method, the solution is numerically implemented considering a more realistic situation: an ultrasonic array with sixteen elements, including a piezocomposite plate, a rear medium and a front matching layer.

5. Application to multi-element transducers

A linear array comprised of sixteen elements is considered. One element is depicted in Fig. 10. The electroactive plate of thickness t = 1 mm is a piezocomposite with 50% piezoelectric material (Pz26) and 50% epoxy resin 1 (ρ = 1673 kg.m^{-3}, E = 4.10^9 Pa, ν = 0.4). Each element of size d = 2 a = 0.66 mm is made of two periods of piezocomposite. On the upper side the electrode is full and grounded. It is covered by a matching layer made of epoxy resin 2 of a quarter wavelength in thickness (t_1 = 0.21 mm. The thickness of the electrode is neglected. On the rear side of the piezocomposite bounded by a backing medium of thickness t_2 = 2 mm made of epoxy resin 3, a partial electrode connects de piezoelectric rods. Material parameters of resins 2 and 3 used in the computations can be found in [33]. Finally, a PML layer allows to absorb all outgoing waves from the bottom wall of the backing medium. Three cases are considered: the reference configuration with floating potential at the rear side, a standard mechanical decoupling configuration with 90% deep slots on left and right (width = a/10) and the new electrical decoupling configuration with an inductive shunt on the rear electrode. In a first step, the dispersion curves for infinite media are shown and commented. In a second step, the radiation diagrams are compared to each other.

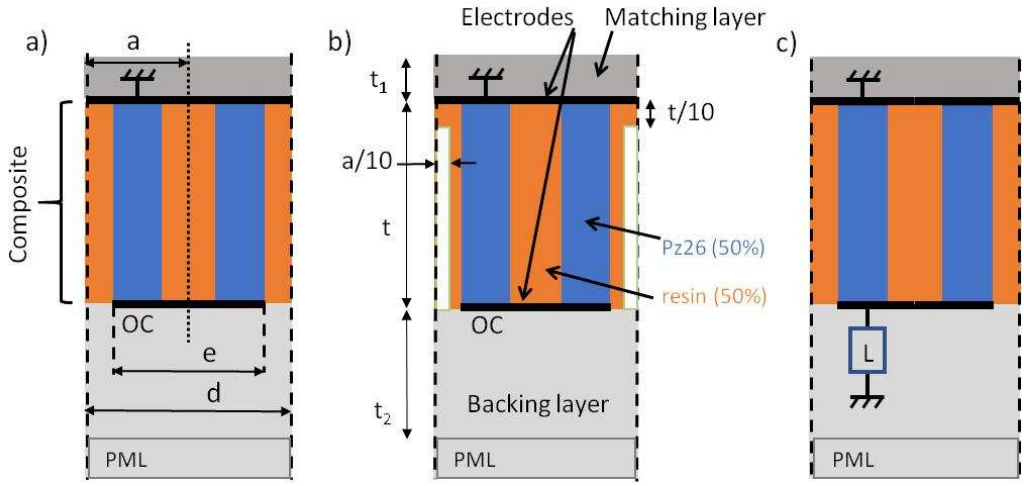

Figure 10: Unit cell model of the infinite piezocomposite plate (a) with open circuit, (b) with mechanical decoupling between the elements and (c) with inductive shunt.

The dispersion curves are shown for each configuration (on the right in Fig. 11(a)-(c)). Calculations are also performed without matching layer nor a backing medium in order to better observe their effect (on the left in Fig. 11(a)-(c)). In the piezocomposite simple plate (Fig. 11(a) left), the thickness resonance frequency is identified at f_r = 1.8 MHz and k = 0 m^{-1}. It corresponds to the cut-off frequency of a one only guided mode in the frequency range 1.5-2 MHz. The S_2 mode is slightly dispersive due to the periodicity of the material. The whole guided modes are affected in different ways according to the decoupling method. The mechanical decoupling effect is mainly observed in the slowdown of the guided mode group velocities whereas for the inductive shunt, a band gap is created at the vicinity of f_r for low k values (left in Fig. 11(b) and 11(c), respectively).

When a matching layer and a backing medium are set, the dispersion curves are changed dramatically. Multiple guided modes and their folding are observed in the three-layer system with the sandwiched piezocomposite simple plate (Fig. 11(a) right). For the case of the central layer with regular cuts (Fig. 11(b) right), most of the guided mode have a weak group velocity and the remaining dispersive modes were observed in the absence of a matching layer and a backing layer. Finally, the third case does not highlight any stop band near the resonance frequency. Nevertheless, the use of inductive shunts reduces the number of guided modes in the trilayer structure (Fig. 11(c) right).

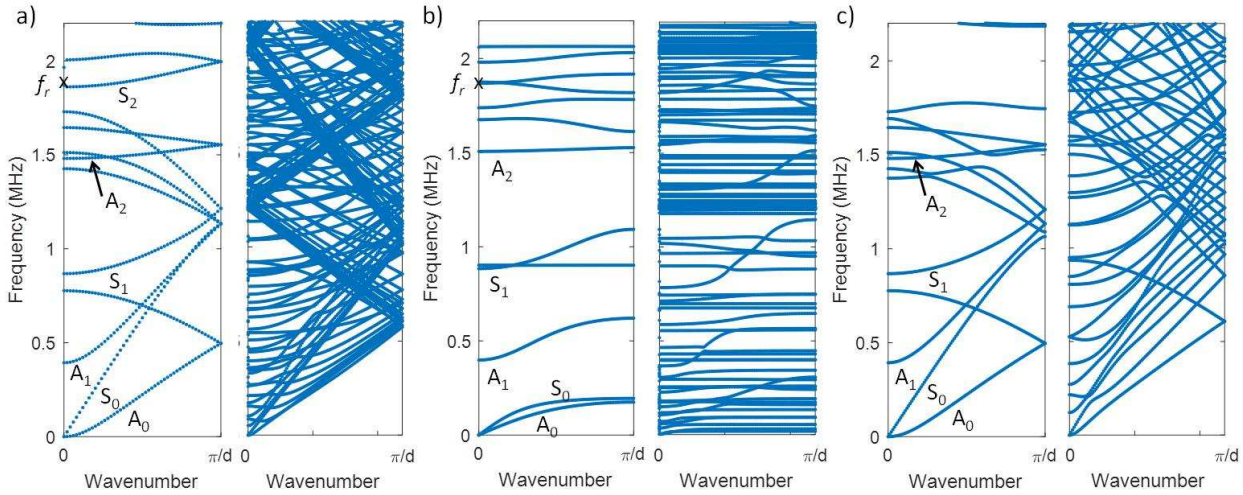

Figure 11: Dispersion curves of the Lamb waves in the piezocomposite transducer: (a) OC boundary condition, (b) with mechanical decoupling between the elements and (c) with IS at the electrical boundary of the passive elements. Without (left) and with (right) front matching layer and backing medium.

In the vicinity of the thickness mode frequency, the dispersion curves of the three-layer systems show significant differences. The influence of the later on the radiated pressure in water is now studied. The radiation pattern for an array comprised of sixteen elements is numerically evaluated for each configuration at the frequency f_r, from the normal displacement field calculated on the upper side of the matching layer. The active element is nearly at the center of the array (red colored sector in Fig. 12(a)). The other elements are either let to floating potential or grounded by an inductive shunt in the last case. Each pattern is normalized by the pressure value at 0°. In the absence of mechanical cutting and shunting, the diagram exhibit broad lateral lobes at ±40° due to multimode propagation and a main lobe of ±18° at -3 dB (blue line). The mechanical decoupling smoothes the whole diagram: the central lobe width reaches at ±53° at -3 dB and secondary lobes are not observable (purple line). Finally, our solution gives intermediate results (red line): when compared to the first case, the main lobe is broadened up to ±22° at -3dB and secondary lobes around ±40° are lowered by 4 dB approximately, due to the lower guided mode density.

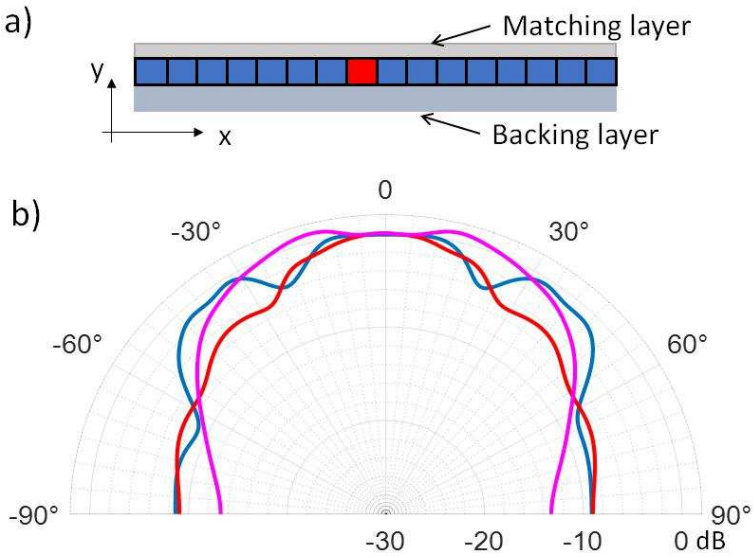

Figure 12: (a) Two-dimensional model of the piezocomposite transducer with 16 elements. The active sector in red is excited by a harmonic voltage source at f_r. (b) Radiation patterns from the piezocomposite transducer at the resonance frequency: OC boundary condition (blue line), with mechanical decoupling between the elements (purple line) and with IS at the electrical boundary of the passive elements (red line).

The results show the possibility of reducing the crosstalk effect by taking advantage of the shunt condition applied to the electrical boundaries of the ultrasonic array. It could therefore be interesting to combine the benefit of decoupling obtained by applying appropriate electrical conditions to the electrodes with that of the physical cutting of the ceramic. In doing so, a technical challenge to come will be on the way to achieve switching between both electrical terminations depending on the type of shunt in view of characteristics required for impedance matching and pass band requirement. This aspect goes beyond the scope of this work and is not further developed here.

6. Conclusion

In this paper, the crosstalk reduction effect by connecting an inductive shunt to passive elements of a piezoelectric phononic plate is investigated. A band gap is opened in the first Brillouin zone, at and at the vicinity of the S_2 mode cut-off frequency which is the resonance frequency of the first thickness mode in the plate when in open circuit condition. Furthermore, no guided mode whose speed is lower than that of water (surrounding environment) is observed.

Inductive shunts have the effect of minimizing the whole field of normal displacements along the plate and localizing them more in the vicinity of the active element. In the radiation pattern for an active element, the angular width of the main lobe is widened by a factor of more than four, which corresponds to a reduction of the effective width of the radiating element by a factor of more than six compared to the open circuit condition. It is interesting to note that these results are maintained if we have only four shunted sectors on either side of the active sector.

The effect of the shunt is closely related to the properties of the sample. In particular, the variation of the electrode coverage rate of a sector (e/a), as well as the presence of an external fluid, will be able to change the results significantly. These studies may be the subject of future developments.

Using inductive shunts settles a resonant effect for each sector that bounds crosstalk reduction over a narrow frequency range. Nevertheless, this study highlights the new and efficient opportunities that arise from connecting circuits to the electrical boundaries of the electroactive plate. The last part of this study addresses the situation of a more realistic ultrasonic array. On one hand, it highlights that the physical effects at the origin of the crosstalk reduction using periodic inductive shunts are different from those inherent to the cutting of a piezocomposite ceramic. On the other hand, the targeted effects are kept including a rear medium and a front matching layer.

From there on, to obtain a wider frequency band as required for applications such as ultrasound imaging, other components (e.g., introducing negative capacitances) or tailored electrical transmission lines to be coupled with the phononic plate have to be used [23, 34-35]. Moreover, it would be advantageous to combine this approach with the usual mechanical dicing techniques used in commercial probes.

7. References

[1] D.H. Turnbull, F.S. Foster, Fabrication and Characterization of Transducer Elements in Two-Dimensional Arrays for Medical Ultrasound Imaging, IEEE Trans. Ultrason. Ferroelectr. Freq. Control. 39 (1992) 464–475. https://doi.org/10.1109/58.148536.

[2] K.K. Shung, M.J. Zipparo, Ultrasonic transducers and arrays, IEEE Eng. Med. Biol. Mag. 15 (1996) 20–30. https://doi.org/10.1109/51.544509.

[3] B.W. Drinkwater, P.D. Wilcox, Ultrasonic arrays for non-destructive evaluation: A review, NDT E Int. 39 (2006) 525–541. https://doi.org/10.1016/j.ndteint.2006.03.006.

[4] L. Merabet, S. Robert, C. Prada, The multi-mode plane wave imaging in the Fourier domain: Theory and applications to fast ultrasound imaging of cracks, NDT E Int. (2019) 102171. https://doi.org/10.1016/j.ndteint.2019.102171.

[5] J. Chang, Z. Chen, Y. Huang, Y. Li, X. Zeng, C. Lu, Flexible ultrasonic array for breast-cancer diagnosis based on a self-shape–estimation algorithm, Ultrasonics 108 (2020) 106199
[6] T. Latête, B. Gauthier, P. Belanger, Towards using convolutional neural network to locate, identify and sizedefects in phased array ultrasonic testing, Ultrasonics 115 (2021) 106436
[7] K.J. Opieliński, M. Celmer, R. Bolejko, Crosstalk Effect in Medical Ultrasound Tomography Imaging, Proc. 2018 Jt. Conf. - Acoust. Acoust. 2018. (2018) 230–235. https://doi.org/10.1109/ACOUSTICS.2018.8502426.
[8] M. Celmer, K.J. Opieliński, M. Dopierała, Structural model of standard ultrasonic transducer array developed for FEM analysis of mechanical crosstalk, Ultrasonics. 83 (2018) 114–119. https://doi.org/10.1016/j.ultras.2017.06.006.
[9] J. Guyonvarch, D. Certon, L. Ratsimandresey, F. Patat, M. Lethiecq, Analytical 2D model of transducer arrays for predicting elementary electroacoustic reponse and directivity pattern, IEEE Int. Ultrason. Symp. IUS. 00 (2002) 1217–1220. https://doi.org/10.1109/ULTSYM.2002.1192513.
[10] M. Phamthi, H. Le Khanh, Fabrication and Characterization of Large Area 1-3 Piezo-composites based on PMN-PT Single Crystals for Transducer Applications, (2009) 1745–1748. https://doi.org/10.1109/ULTSYM.2009.5441989.
[11] W.A. Smith, Role of piezocomposites in ultrasonic transducers, Ultrason. Symp. Proc. 2 (1989) 755–766. https://doi.org/10.1109/ultsym.1989.67088.
[12] A. Bybi, C. Granger, S. Grondel, A. Hladky-hennion, J. Assaad, NDT & E International Electrical method for crosstalk cancellation in transducer arrays, NDT E Int. 62 (2014) 115–121. https://doi.org/10.1016/j.ndteint.2013.12.003.
[13] I. Laasri, A. Bybi, O. Mouhat, M. Jamal, A.C. Hladky, A. Ettahir, K. Kettani, Investigation of the electrical limit conditions effects in piezoelectric transducer arrays utilized in medical imaging, Appl. Acoust. 170 (2020) 107509. https://doi.org/10.1016/j.apacoust.2020.107509.
[14] C.E. Morton, G.R. Lockwood, Evaluation of kerfless linear arrays, Proc. IEEE Ultrason. Symp. 2 (2002) 1257–1260. https://doi.org/10.1109/ultsym.2002.1192522.
[15] C.E.M. Démoré, S. Cochran, J.C. Bamber, 1-3 Piezocomposite Design Optimised for High Frequency Kerfless Transducer Arrays, (2009). https://doi.org/10.1109/ULTSYM.2009.0275.
[16] H.L.W. Chan, J. Unsworth, Simple Model for Piezoelectric Ceramic / Polymer 1-3 Composites Used in Ultrasonic Transducer Applications, (1989) 434–441. https://doi.org/10.1109/58.31780.
[17] K.S. Ramadan, D. Sameoto, S. Evoy, A review of piezoelectric polymers as functional materials for electromechanical transducers, Smart Mater. Struct. 23 (2014). https://doi.org/10.1088/0964-1726/23/3/033001.
[18] N. Aravantinos-Zafirisa, F. Lucklumb, M. M. Sigalas, Complete phononic band gaps in the 3D Yablonovite structure with spheres, Ultrasonics 110 (2021) 106265
[19] A. Trzaskowskaa, P. Hakonenb, M. Wiesnera, S. Mielcarek, Generation of a mode in phononic crystal based on 1D/2D structures, Ultrasonics 106 (2020) 106146
[20] S.A. Mansoura, P. Maréchal, B. Morvan, B. Dubus, Active control of a piezoelectric phononic crystal using electrical impedance, (2014) 951–954. https://doi.org/10.1109/ULTSYM.2014.0233.
[21] C. Vasseur, C. Croenne, B. Dubus, J. Vasseur, A.C. Hladky-Hennion, C. Prevot, P. Martins, M. Pham-Thi, Numerical and experimental demonstration of the electrical Bragg band gaps in piezoelectric plates with a periodic array of electrodes, IEEE Int. Ultrason. Symp. IUS. (2017) 0–3. https://doi.org/10.1109/ULTSYM.2017.8092676.
[22] N. Kherraz, L. Haumesser, F. Levassort, P. Benard, B. Morvan, Hybridization bandgap induced by an electrical resonance in piezoelectric metamaterial plates, J. Appl. Phys. 123 (2018). https://doi.org/10.1063/1.5016496.
[23] N. Kherraz, F.-H. Chikh-Bled, R. Sainidou, B. Morvan, P. Rembert, Tunable phononic structures using Lamb waves in a piezoceramic plate, 094302 (2019) 1–12. https://doi.org/10.1103/PhysRevB.99.094302.
[24] S. Degraeve, C. Granger, B. Dubus, J.O. Vasseur, M. Pham Thi, A.C. Hladky-Hennion, Bragg band gaps tunability in an homogeneous piezoelectric rod with periodic electrical boundary conditions, J. Appl. Phys. 115 (2014). https://doi.org/10.1063/1.4876757.
[25] N. Kherraz, Contrôle de la propagation d'ondes guidées dans une plaque piézoélectrique par application de conditions aux limites électriques périodiques, Thesis. (2017). https://tel.archives-ouvertes.fr/tel-01617398/.
[26] C. Hakoda, J. Rose, P. Shokouhi, C. Lissenden, C. Hakoda, J. Rose, P. Shokouhi, Using Floquet

Periodicity to Easily Calculate Dispersion Curves and Wave Structures of Homogeneous Waveguides, 020016 (2018). https://doi.org/10.1063/1.5031513.
[27] S. Sherrit, S.P. Leary, B.P. Dolgin, Y. Bar-Cohen, Comparison of the Mason and KLM equivalent circuits for piezoelectric resonators in the thickness mode, Proc. IEEE Ultrason. Symp. 2 (1999) 921–926. https://doi.org/10.1109/ultsym.1999.849139.
[28] D. Royer, E. Dieulesaint, Ondes élastiques dans les solides - Tome 2, Chapter 6, (2000). http://archives.umc.edu.dz/handle/123456789/119070.
[29] D. Certon, G. Ferin, O. Bou Matar, J. Guyonvarch, J.P. Remenieras, F. Patat, Influence of acousto-optic interactions on the determination of the diffracted field by an array obtained from displacement measurements, Ultrasonics. 42 (2004) 465–471. https://doi.org/10.1016/j.ultras.2003.12.035.
[30] B. Delannoy, H. Lasota, C. Bruneel, R. Torguet, E. Bridoux, The infinite planar baffles problem in acoustic radiation and its experimental verification, J. Appl. Phys. 50 (1979) 5189–5195. https://doi.org/10.1063/1.326656.
[31] J. Assaad, C. Bruneel, Radiation from finite phased and focused linear array including interaction, 101 (1997) 1859–1867. https://doi.org/10.1121/1.418237.
[32] N. Felix, D. Certon, E. Lacaze, M. Lethiecq, F. Patat, Experimental investigation of cross-coupling and its influence on the elementary radiation pattern in 1D ultrasound arrays, Proc. IEEE Ultrason. Symp. 2 (1999) 1053–1056. https://doi.org/10.1109/ULTSYM.1999.849181.
[33] D. Certon, J. Guyonvarch, G. Ferin, F. Patat, Two-dimensional electroacoustic model of transducer array based on 1-3 piezocomposite materials, IEEE TUFFC, 53 (12), (2006), 2471-2480.
[34] Y. Lu, J. Tang, Electromechanical tailoring of structure with periodic piezoelectric circuitry, J. Sound Vib. 331 (2012) 3371–3385. https://doi.org/10.1016/j.jsv.2012.02.029.
[35] A.E. Bergamini, M. Zündel, E.A. Flores Parra, T. Delpero, M. Ruzzene, P. Ermanni, Hybrid dispersive media with controllable wave propagation: A new take on smart materials, J. Appl. Phys. 118 (2015). https://doi.org/10.1063/1.4934202.